Conf-900147--1

Heavy Ion Inelastic Scattering with a 4π Gamma Detector

E. E. Gross
Oak Ridge National Laboratory
Oak Ridge, Tennessee 37831-6368 U.S.A.

CONF-900147--1

DE90 002709

ABSTRACT

Heavy-ion inelastic scattering with a new technique that uses a 4 π γ-ray detector in coincidence with charged particle detectors is applied to ^{24}Mg(200 MeV) + ^{208}Pb scattering. In addition to differential cross sections, a complete particle-γ angular correlation is obtained for decay of the 2_1^+ (1.37 MeV) state of ^{24}Mg. The data are analyzed in coupled-channels. The correlation data proves to be especially sensitive to the static quadrupole moment.

I. INTRODUCTION

Inelastic scattering has proven itself to be a valuable source of nuclear structure information by providing the energies, spins, parities, and transition rates for nuclear levels. Such information has spurred the development of nuclear structure models such as the shell model, the collective model, the potential energy surface model, etc., and continues to provide testing ground for theory. In this manner the E2 systematics of the lowest 2^+ state of even-even nuclei[1] has been constructed over the years and has proven to be useful in establishing closed shell regions and regions of high deformation.

The E4 systematics to the lowest 4^+ states of even-even nuclei are much less well established. Where reliable data on hexadecapole moments do exist, they have proven valuable in providing nuclear shape information for sensitive testing of nuclear structure models.[2,3] Determination of hexadecapole moments requires absolute measurements of the direct excitation of 4_1^+ states from 0_1^+ ground states, but data are hard to obtain by heavy-ion scattering because the cross sections are low and because there are severe difficulties, except for the lightest elements, in resolving the 4_1^+ state from neighboring states using conventional particle detection techniques. To overcome some of these difficulties, we have resorted to a new technique[4] which employs a nearly 4π γ-ray detector, the Spin Spectrometer,[5] to obtain the necessary resolution, with high γ-ray efficiency, in coincidence with solid state particle detectors which provide the information for the differential cross sections. If the γ-ray detector is segmented, as is the 72 detector Spin Spectrometer, this technique then has the added feature of providing particle-γ correlation information. Here we report on applying the technique to levels in ^{24}Mg excited by 200 MeV ^{24}Mg ions scattered from a ^{208}Pb target. The beam energy was chosen to provide data in the Coulomb-nuclear interference region where absolute normalization was provided by Rutherford scattering at the forward angles and the interference region provided sensitivity to signs as well as to magnitudes of the matrix elements.

II. DIFFERENTIAL CROSS SECTIONS

Experimental details are contained in ref. 4. Let it suffice to say that, for the NaI detectors used, the Doppler shift effect made it possible to separate the 4_1^+(4.12 MeV) and 2_2^+(4.24 MeV) states in ^{24}Mg from overlapping decay γ's from ^{208}Pb. This separation was only possible for a selection of NaI detectors (about 30% of 4π) located along the ^{24}Mg recoil direction. This was enough to establish differential cross sections for these states but not enough to obtain reliable tensor alignments. The first 2^+ state of ^{24}Mg (1.37 MeV) was easily resolved in all detectors and a complete tensor alignment was obtained.

The differential cross sections for elastic scattering and for the inelastic excitation of the 2_1^+(1.37 MeV), 4_1^+(4.12 MeV), and 2_2^+(4.24 MeV) states in ^{24}Mg resulting from 200 MeV ^{24}Mg + ^{208}Pb reactions are shown in Figs. 1-4. The 200 MeV ^{24}Mg beam was provided by the 25 MV tandem of the ORNL Holifield Heavy Ion Facility. Also shown on the figures, as solid curves, are the coupled channels fits to the differential cross sections. These fits result from a minimization of total χ^2 by variation of a six-parameter deformed optical potential and the 13 matrix elements connecting the states. The calculations were performed using the symmetric rotor model option of the program ECIS.[6]

A. The 2_1+(1.37 MeV) State

The fit to this state is a delicate balance between the basic E2 matrix element, M(E2;$0_1^+ \leftrightarrow 2_1^+$), and the E2 reorientation matrix element for the state, M(E2;$2_1^+ \leftrightarrow 2_1^+$). This is illustrated in Fig. 2 where the dotted curve shows what happens to the best fit when the reorientation matrix element is set to zero. Evidently, reorientation affects the differential cross section over the entire angular range although its effect on χ^2 is most pronounced at back angles. The interplay between the two matrix elements is also illustrated in Fig. 5a which shows the χ^2 behavior as a function of $M(E2;2_1^+\leftrightarrow 2_1^+)$, expressed as a static quadrupole moment, for various values of $M(E2;0_1^+\leftrightarrow 2_1^+)$. On the basis of fitting the differential cross section only, values of $M(E2;0_1^+\leftrightarrow 2_1^+) = (-20.4 \pm 0.3)$ e fm^2 and $Q_2 = (+20 \pm 4)$ e fm^2 would be preferred.

B. The 4_1^+(4.12 MeV) State

Although the dominant excitation to the 4_1^+ state is via double E2 excitation, the data of Fig. 3 contain a significant sensitivity to direct E4 excitation. This is illustrated by the dashed curve which is the best fit to our data that can be obtained with the electron scattering value[7] for the basic E4 matrix element, $M(E4;0_1^+\leftrightarrow 4_1^+) = 41$ e fm^4. The best fit to our data, the solid curve, is for a value $M(E4;0_1^+\leftrightarrow 4_1^+) = (142 \pm 9)$ e fm^4. The dotted curve shows the effect of adding the 6_1^+ state at 8.11 MeV to the analysis.

C. The 2_2^+(4.24 MeV) State

The solid curve in Fig. 4 is the best fit to the second 2^+ state using symmetric rotor model form factors. A natural way to account for this state is by postulating a triaxial shape for ^{24}Mg. The best asymmetric rotor model[8] fit to the 2_2^+ state is shown as the long dashed curve in Fig. 4 and is for a value of 8.5° for the γ parameter of the theory. However, from the level spacings of the two 2^+ states, the value of γ should be 22°. A further apparent failure of the asymmetric-rotor model for ^{24}Mg is the prediction that the product of the three matrix elements $p_3 = M(E2;0_1\leftrightarrow 2_1)\, M(E2;0_1\leftrightarrow 2_2)\, M(E2;2_1\leftrightarrow 2_2)$ is less than zero whereas the fit to the data utilizing symmetric-rotor model form-factors, the solid curve in Fig. 4, requires this product to be positive. Shell model calculations[9] also predict $p_3 > 0$. The short dotted curve illustrates the effect of using γ-decay values[10] for $M(E2;0 \leftrightarrow 2_2)$ and $M(E2;2_1 \leftrightarrow 2_2)$ matrix elements with signs consistent with shell model predictions.[9]

III. ALIGNMENT TENSORS

Here we make use of the discrete nature of the Spin Spectrometer and extract the perturbed γ-ray angular correlation for the first 2^+ state (1.37 MeV) of ^{24}Mg, expressed in terms of alignment tensors, t_{kq}, from the response of individual NaI detectors. The angular distribution for the $2_1{}^+ \rightarrow 0_1{}^+$ γ-ray, neglecting cascades from higher states, is given by:

$$\frac{dW(\theta_\gamma, \phi_\gamma, \gamma_{2_1 \rightarrow 0_1})}{d\Omega_\gamma} = \frac{1}{4\pi} \left\{ 1 + \frac{\sqrt{4\pi}}{t_{00}} \sum_{\substack{k=2,4 \\ -k \leq q \leq k}} t_{kq} F_k(2,2,0,2) Y_{kq}(\theta,\phi) \right\}$$

The F_k are tabulated γ-γ correlation coefficients[11] and the t_{kq} are the statistical tensors for populating the $2_1{}^+$ state. We choose a lab coordinate system where θ and φ are the polar and azimuthal angles of the detected γ-ray with respect to a z-axis along the recoil ^{24}Mg direction. In fitting this expression to the observed γ-ray angular correlation, we account for the attenuation due to the finite solid angle of each detector. The resulting experimental alignment tensors are shown as data points in Figs. 6-9.

To compare with the experimental alignment tensors, we adjust the calculated alignment tensors for the attenuation due to the hyperfine precession of the recoiling $^{24}\mathrm{Mg}^{11+}$ ions before the γ-ray is emitted.[12] The alignment tensors represented by the above fit to the differential cross section data, and corrected for hyperfine attenuation, are shown by the dashed curves and compared to the measured tensors in Figs. 6-9. There are two features to be noted about this comparison. First, the calculation reproduces the general trends of the measured alignment tensors and there is remarkable agreement in the Coulomb dominated region, $\theta_{cm} < 40°$. Secondly, in spite of the excellent coupled channels fits to the differential cross sections, there is considerable room for improvement in the predicted behavior of the alignment tensors at large angles. Sensitivity of the alignment tensors to the nuclear optical potential was investigated by calculations using the shallow and the deep potentials of ref. 4. Both potentials give identical alignment tensors. *Sensitivity of the alignment tensors to the* $M(E4;\ 0_1 \leftrightarrow 4_1)$ *matrix element* was also investigated. For values 41 efm^4 ≤ $M(E4;\ 0_1 \leftrightarrow 4_1)$ ≤ 142 efm^4, there is no sensitivity provided $M(E2;\ 0_1 \leftrightarrow 2_1)$ is adjusted to maintain the fit to the 2^{1+} differential cross section. This range of $M(E4;\ 0^2 \leftrightarrow 4^1)$ covers the range of reported values.[4,7]

All the sensitivity to the large-angle alignment tensors appears to reside in the E2 reorientation matrix element $M(E2;\ 2_1 \leftrightarrow 2_1) = 1.32\ Q_2$. The above $0^+ \leftrightarrow 2^+ \leftrightarrow 4^+$ coupled channels rotational-model calculations were repeated but now including the $2_1{}^+$ alignment tensors in the calculation of χ^2. The eight alignment tensors were considered as a single alignment determination at each angle and therefore weighted as a single data point on a par with the differential cross section measurements at that angle. The χ^2 surfaces explored in this manner are shown in Fig. 5b for the alignment tensors and Fig. 5c for the sum of χ^2 for fitting the tensors and the $2_1{}^+$ differential cross section. Figure 5b shows that the alignment tensors prefer $Q_2 \approx +32$ efm^2 irrespective of the value of ME2. Figure 5c indicates that a good compromise between fitting the $2_1{}^+$ differential cross section and the $2_1{}^+$ alignment tensors is $Q_2 =$ (+30 ± 4) efm^2 and $M(E2;0_1 \leftrightarrow 2_1) = (-20.6 \pm 0.3)$ efm^2. With these values, the χ^2 for the fit to the $2_1{}^+$ differential cross section has increased by about 15% over the best fit, almost indistinguishable from the solid curve in Fig. 2. However, as these values account for a larger body of data, they must be considered as more reliable than the values obtained by fitting the differential cross sections alone. As the resulting static quadrupole moment is some 60% ± 20% larger than the rigid rotor value, this is a problem for theory[9,13,14] which prefers values close to the rigid rotor value.

DISCLAIMER

IV. ACKNOWLEDGEMENTS

The experiments were carried out by D. C. Hensley, J. R. Beene, F. E. Bertrand, M. L. Halbert, D. L. Humphrey, T. VanCleve and G. Vourvopoulos. The research at Oak Ridge National Laboratory was sponsored by the Division of Nuclear Physics, U. S. Department of Energy, under Contract DE-AC05-84OR21400 with Martin Marietta Energy Systems, Inc.

REFERENCES

1. S. Raman, C.H. Malarkey, W.T. Milner, C.W. Nestor, and P.H. Stelson, Atom. and Nucl. Data Tables 36, 1 (1987).
2. E. Eichler, N.R. Johnson, R.O. Sayer, D.C. Hensley, and L.L. Riedinger, Phys. Rev. Lett. 30, 568 (1973).
3. F. Todd Baker, Alan Scott, T.P. Cleary, J.L.C. Ford, E.E. Gross, and D.C. Hensley, Nucl. Phys. A321, 222 (1979).
4. D.C. Hensley, E.E. Gross, M.L. Halbert, J.R. Beene, F.E. Bertrand, G. Vourvopoulos, D.L. Humphrey, and T. VanCleve, Phys. Rev. C, to be published.
5. M. Jaaskelainen, D.G. Sarantites, R. Woodward, F. A. Dilmanian, J.T. Hood, R. Jaaskelainen, D.C. Hensley, M.L. Halbert, and J.H. Barker, Nucl. Instrum. Methods 204, 385 (1983).
6. J. Raynal, Phys. Rev. C 23, 2571 (1981).
7. Y. Horikawa, Y. Torizuka, A. Nakada, S. Mitsunobu, Y. Kojima, and M. Kimura, Phys. Lett. 36B, 9 (1971).
8. A.S. Davydov and G.F. Filippov, Nucl. Phys. 8, 237 (1958).
9. J.B. McGrory, private communication.
10. P.M. Endt and C. van der Leun, Nucl. Phys. A214, 1 (1973).
11. H.J. Rose and D.M. Brink, Rev. Mod. Phys. 39, 306 (1967).
12. Z. Berant, M.B. Goldberg, G. Goldring, S.S. Hanna, H.M. Loebenstein, I. Plesser, M. Popp, J.S. Sokolowski, P.N. Tandon, and Y. Wolfson, Nucl. Phys. A178, 155 (1971).
13. Y. Abgrall, B. Morand, and E. Caurier, Nucl. Phys. A192, 372 (1972).
14. M.R. Gunye, Phys. Lett. 37B, 125 (1971).

FIGURE CAPTIONS

Fig. 1. ^{24}Mg (200 MeV) + ^{208}Pb elastic scattering relative to Rutherford scattering. The solid curve represents our best fit from a $0_1 \leftrightarrow 2_1 \leftrightarrow 4_1 \leftrightarrow 2_2$ symmetric-rotor coupled-channels analysis.

Fig. 2. Differential cross section for exciting the ^{24}Mg 2_1 state (1.37 MeV) by 200 MeV ^{24}Mg scattering from ^{208}Pb. The solid curve represents our best fit from a $0_1 \leftrightarrow 2_1 \leftrightarrow 4_1 \leftrightarrow 2_2$ symmetric-rotor coupled-channels analysis. The dotted curve shows what happens to this calculation when the static quadrupole moment is set to zero.

Fig. 3. Differential cross section for exciting the ^{24}Mg 4_1 state (4.12 MeV) by 200 MeV ^{24}Mg scattering from ^{208}Pb. The solid curve represents our best fit from a $0_1 \leftrightarrow 2_1 \leftrightarrow 4_1 \leftrightarrow 2_2$ symmetric-rotor coupled-channels analysis. The dotted curve shows the effect on the 4_1 state of including the 6_1 state (8.11 MeV) in the calculation. The dashed curve shows the effect of decreasing the $M(E4;0_1 \leftrightarrow 4_1)$ matrix element from the best fit value (solid curve) of 142 e fm^4 to the electron scattering value of 41 e fm^4.

Fig. 4. Differential cross section for exciting the ^{24}Mg 2_2 state (4.24 MeV) by 200 MeV ^{24}Mg scattering from ^{208}Pb. The solid curve represents our best fit from a $0_1 \leftrightarrow 2_1 \leftrightarrow 4_1 \leftrightarrow 2_2$ symmetric-rotor coupled-channels analysis. The dashed curve represents the minimum χ^2 fit by varying the parameter γ_C(=8°) of the asymmetric rotor model. The short dotted curve illustrates the effect of using γ-decay values for $M(E2;0 \leftrightarrow 2_2)$ and $M(E2;2_1 \leftrightarrow 2_2)$ matrix elements with signs consistent with shell model predictions.

Fig. 5. The variation of χ^2 with the static quadrupole moment, Q_2, from coupled-channels fits to (a) the 2_1^+ differential cross section, (b) the 2_1^+ alignment tensors, and (c) the sum of (a) and (b). The triangles are for ME2 = 20.44 e fm^2, the circles for ME2 = 20.60 e fm^2, and the squares are for ME2 = 20.75 e fm^2.

Fig. 6. The circles are measured t_{22} and t_{44} alignment tensors for the decay of ^{24}Mg*(1.37 MeV) excited by 200 MeV ^{24}Mg scattering from ^{208}Pb. The dashed curves are predicted tensors, corrected for hyperfine precession, calculated from coupled-channels fits to the differential cross sections only. The solid curves are the best compromise fit to the sum of the 2_1^+ differential cross section and the alignment tensors.

Fig. 7. The circles are measured t_{20} and t_{21} alignment tensors for *the decay of* ^{24}*Mg***(1.37 MeV) excited by 200 MeV* ^{24}*Mg scattering from* ^{208}Pb. The dashed curves are predicted tensors, corrected for hyperfine precession, calculated from coupled-channels fits to the differential cross sections only. The solid curves are the best compromise fit to the sum of the 2_1^+ differential cross section and the alignment tensors.

Fig. 8. The circles are measured t_{40} and t_{42} alignment tensors for the decay of ^{24}Mg*(1.37 MeV) excited by 200 MeV ^{24}Mg scattering from ^{208}Pb. The dashed curves are predicted tensors, corrected for hyperfine precession, calculated from coupled-channels fits to the differential cross sections only. The solid curves are the best compromise fit to the sum of the 2_1^+ differential cross section and the alignment tensors.

Fig. 9. The circles are measured t_{43} and t_{41} alignment tensors for the decay of ^{24}Mg*(1.37 MeV) excited by 200 MeV ^{24}Mg scattering from ^{208}Pb. The dashed curves are predicted tensors, corrected for hyperfine precession, calculated from coupled-channels fits to the differential cross sections only. The solid curves are the best compromise fit to the sum of the 2_1^+ differential cross section and the alignment tensors.

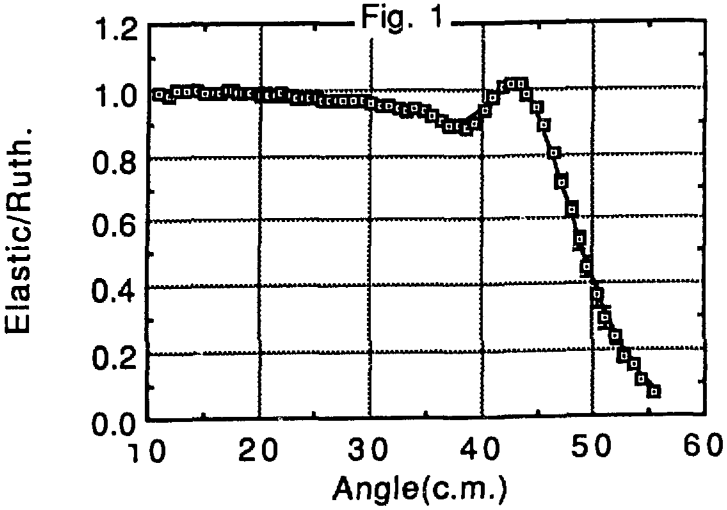
Fig. 1

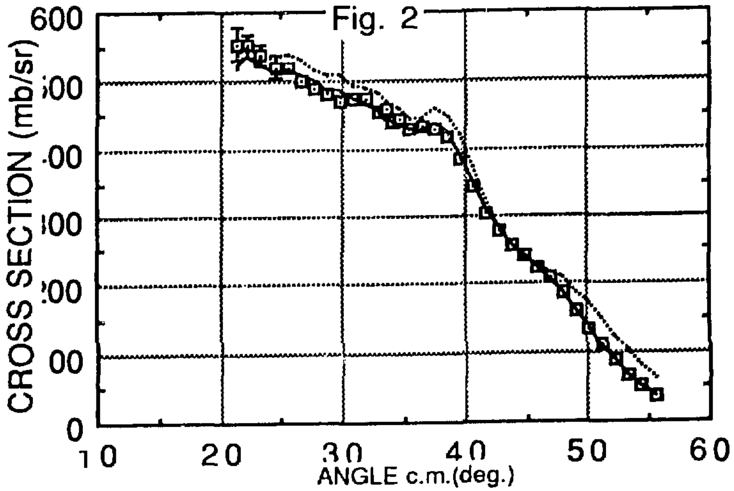
Fig. 2

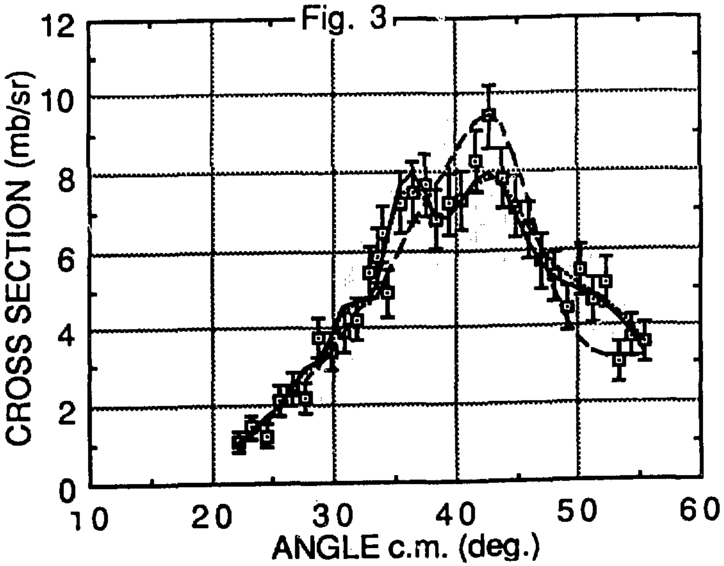
Fig. 3

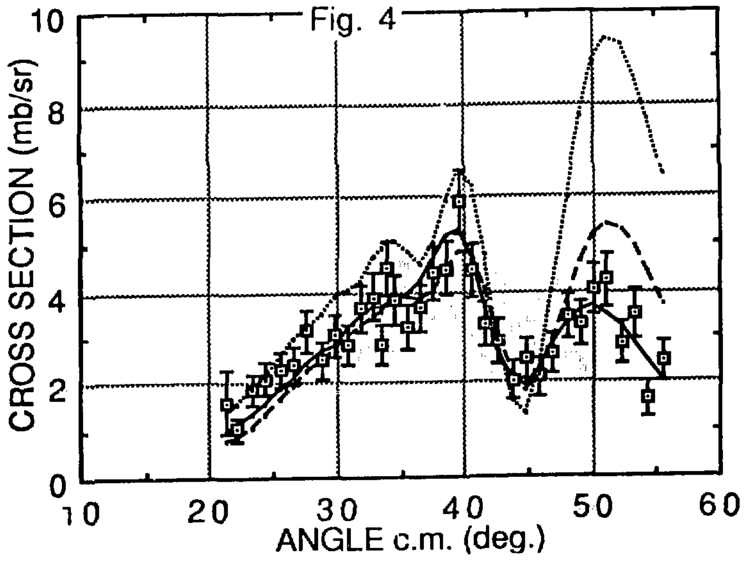
Fig. 4

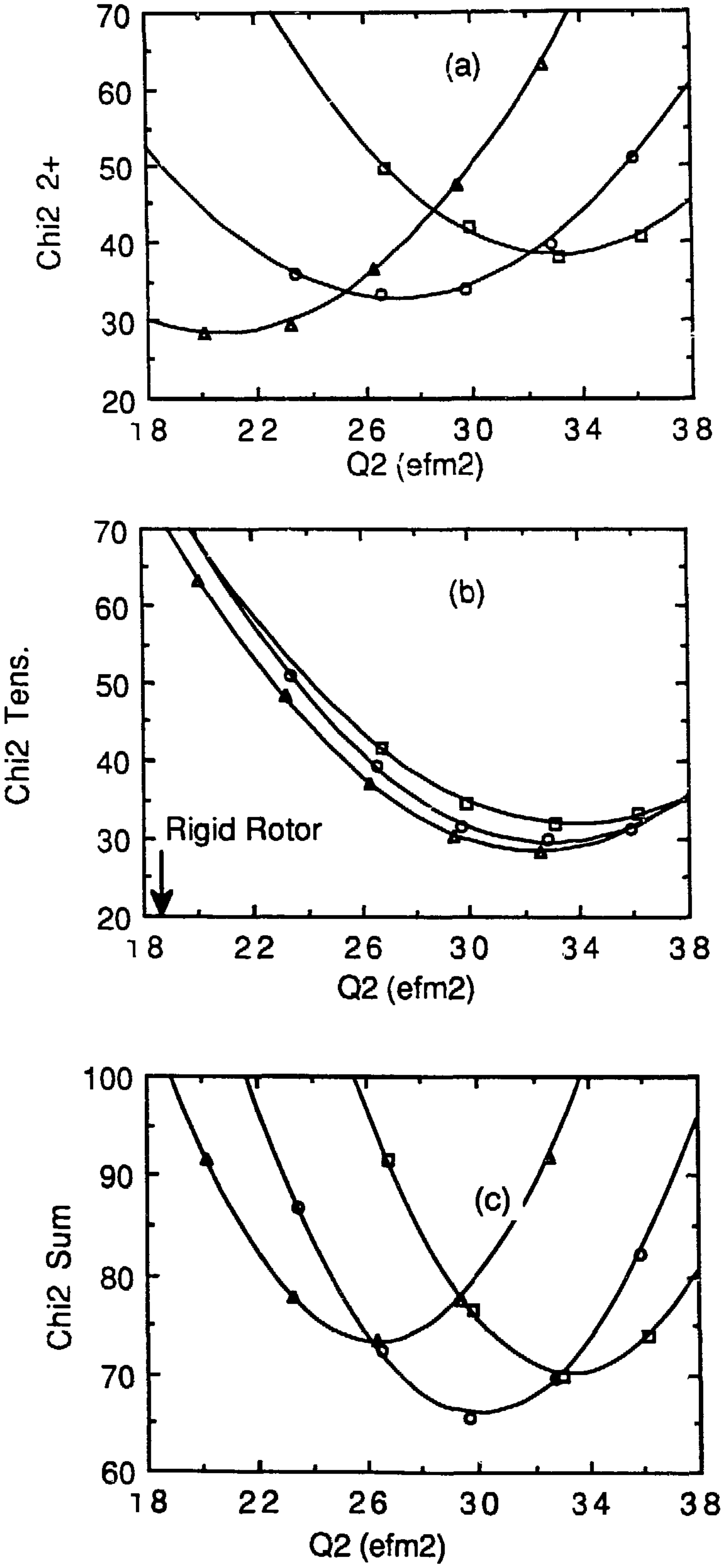
(a)
Chi2 2+
70
60
50
40
30
20
18
22
26
30
34
38
Q2 (efm2)
(b)
Chi2 Tens.
Rigid Rotor
70
60
50
40
30
20
18
22
26
30
34
38
Q2 (efm2)
(c)
Chi2 Sum
100
90
80
70
60
18
22
26
30
34
38
Q2 (efm2)

Fig. 5

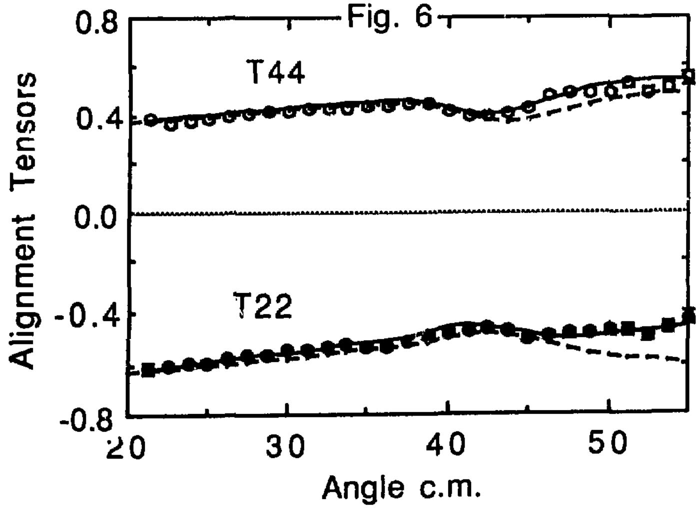
Fig. 6

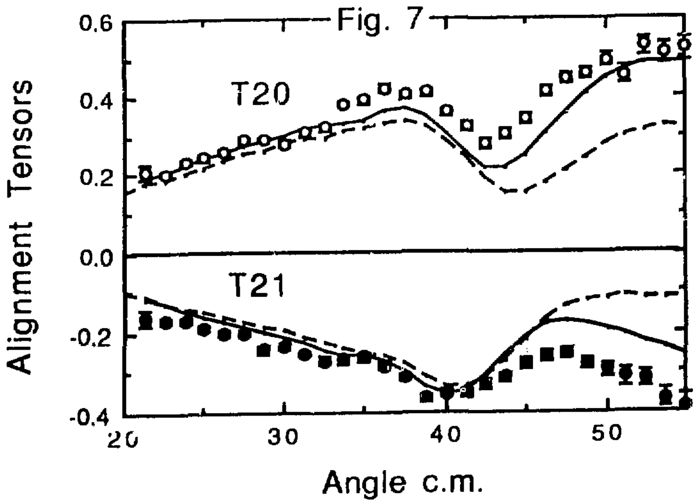
Fig. 7

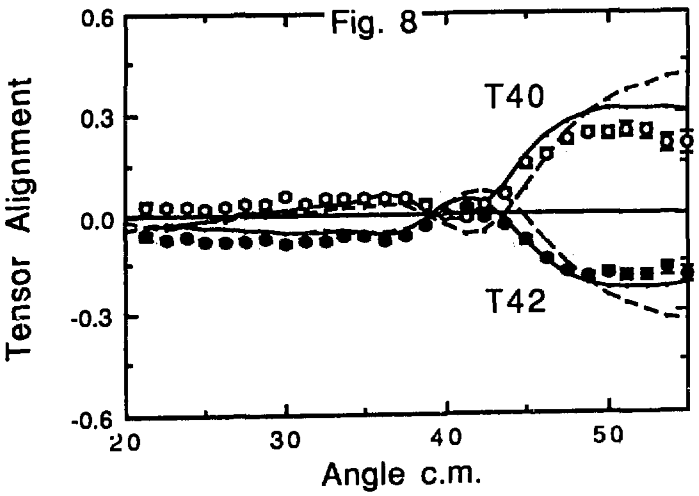
Fig. 8

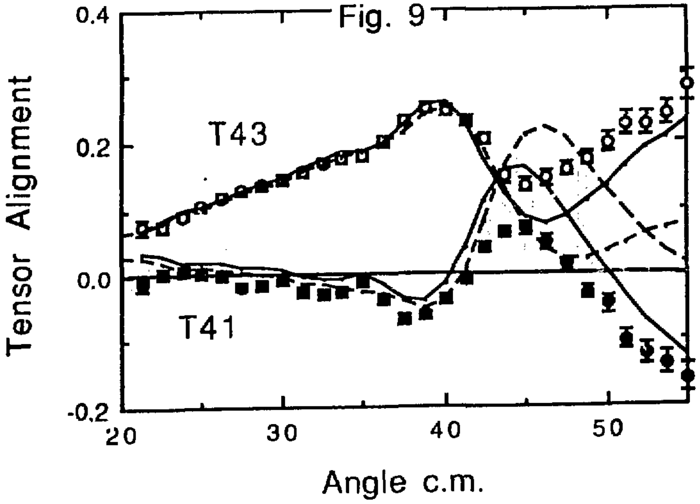
Fig. 9